Astronomy & Astrophysics manuscript no.
(will be inserted by hand later)

Hot HB stars in globular clusters - Physical parameters and consequences for theory. VI. The second parameter pair M 3 and M 13

S. Moehler[1,2*], W.B. Landsman[3], A.V. Sweigart[4], and F. Grundahl[5]

[1] Dr. Remeis-Sternwarte, Astronomisches Institut der Universität Erlangen-Nürnberg, Sternwartstr. 7, 96049 Bamberg, Germany
[2] Institut für Theoretische Physik und Astrophysik, Abteilung Astrophysik, Leibnizstraße 15, 24098 Kiel, Germany (e-mail: moehler@astrophysik.uni-kiel.de)
[3] SSAI, NASA Goddard Space Flight Center, Code 681, Greenbelt, MD 20771, USA (e-mail: landsman@mpb.gsfc.nasa.gov)
[4] NASA Goddard Space Flight Center, Code 681, Greenbelt, MD 20771, USA (e-mail: sweigart@bach.gsfc.nasa.gov),
[5] Institute of Physics and Astronomy, Aarhus University, Ny Munkegade, 8000 Aarhus C, Denmark (e-mail: fgj@ifa.au.dk)

2002/10/4

Abstract. We present the results of spectroscopic analyses of hot horizontal branch (HB) stars in M 13 and M 3, which form a famous "second parameter" pair. From the spectra we derived – for the first time in M 13 – atmospheric parameters (effective temperature and surface gravity) as well as abundances of helium, magnesium, and iron. Consistent with analyses of hot HB stars in other globular clusters we find evidence for helium depletion and iron enrichment in stars hotter than about 12,000 K in both M 3 and M 13. Accounting for the iron enrichment substantially improves the agreement with canonical evolutionary models, although the derived gravities and masses are still somewhat too low. This remaining discrepancy may be an indication that scaled-solar metal-rich model atmospheres do not adequately represent the highly non-solar abundance ratios found in blue HB stars with radiative levitation. We discuss the effects of an enhancement in the envelope helium abundance on the atmospheric parameters of the blue HB stars, as might be caused by deep mixing on the red giant branch or primordial pollution from an earlier generation of intermediate mass asymptotic giant branch stars.

Key words. Stars: atmospheres – Stars: evolution – Stars: horizontal branch – Globular clusters: individual: M 3 – Globular clusters: individual: M 13

1. Introduction

The two globular clusters M 3 and M 13 form a famous "second parameter" pair of clusters that show very different horizontal branch (HB) morphologies despite quite similar metallicities ([Fe/H] = −1.57 for M 3 and −1.54 for M 13, Harris 1996): M 3 possesses a horizontal HB populated from the red to the blue end, while M 13 exhibits a predominantly blue HB followed by a very long blue tail that extends to temperatures of ≈ 35,000 K (Parise et al. 1998). No consensus has yet been reached on the reasons for this difference in HB morphology. While it has often been argued that age, one of the most widely discussed 2nd parameter candidates (Sarajedini et al. 1997), cannot be the 2nd parameter for this pair (Catelan & de Freitas Pacheco 1995, Ferraro et al. 1997, Paltrinieri et al. 1998, Grundahl 1999), the subject remains controversial (e.g. Rey et al. 2001). VandenBerg (2000), in particular, has emphasized that something other than age must be different between M 3 and M 13.

M 13 (along with ω Cen) harbors the most dramatic examples of stars presenting abundance anomalies on the upper red giant branch (RGB; Kraft et al. 1993, 1995, 1997, Cavallo & Nagar 2000), whereas the abundance anomalies in M 3 are considerably less pronounced (Kraft et al. 1992, Cavallo & Nagar 2000). In particular, the super-oxygen poor stars found near the tip of the RGB in M 13 are absent in M 3. These abundance anomalies may arise from deep mixing processes which bring up nu-

Send offprint requests to: S. Moehler

* Based on observations collected at the German-Spanisch Astronomical Center (DSAZ), Calar Alto, operated by the Max-Planck-Institut für Astronomie Heidelberg jointly with the Spanish National Commission for Astronomy

clearly processed material from the vicinity of the hydrogen burning shell during a star's RGB phase. Support for this possibility comes from the larger Na and Al abundances and smaller O and Mg abundances found in stars near the tip of the RGB in M 13 compared to stars further down the RGB (Kraft 1999, Cavallo & Nagar 2000). Alternatively, the recent detections of similar abundance anomalies among main-sequence stars in a few clusters (Cannon et al. 1998, Gratton et al. 2001) suggest a primordial origin, perhaps due to pollution from an earlier generation of intermediate mass asymptotic giant branch (AGB) stars.

Both the deep mixing and primordial scenarios for the origin of the abundance anomalies may have consequences for the luminosity and morphology of the HB, as outlined by Sweigart (1997b) and D'Antona et al. (2002), respectively. Briefly, in the deep-mixing scenario, helium from the H-burning shell is mixed into the envelope on the RGB and thereby causes a star to have a bluer and more luminous position on the HB. In the primordial scenario, stars on the main-sequence which have been polluted by the products of an earlier AGB generation have a higher helium abundance. These polluted stars will then have a lower turnoff mass for a given age than the unpolluted cluster stars with a normal helium abundance, and thus will be more likely to end up on the blue end of the HB. As in the deep-mixing scenario, the primordial scenario also predicts a higher luminosity of the hydrogen shell on the HB, due to the increased helium abundance.

Thus, both the deep mixing and primordial scenarios predict that the stars with the strongest abundance anomalies should end up on the bluest part of the HB, and have both a higher helium abundance and higher luminosity (and lower gravity) than the cooler HB stars. Unfortunately, a straightforward test of these predictions is complicated by the processes of diffusion and radiative levitation in HB stars. The observed photospheric helium abundance in hot HB stars, for example, has long been known to be strongly depleted (see Moehler 2001 for an overview) presumably due to gravitational settling. Moreover, the use of luminosity or gravity discriminants for testing these scenarios is complicated by the recent discovery of supersolar iron abundances in HB stars hotter than $\approx$11,500 K (Behr et al. 1999) due to radiative levitation (Michaud et al. 1983). If the hot HB stars with enhanced abundances are analysed with model atmospheres at the cluster abundance, the stars appear to have anomalously low gravities (Moehler et al. 2000) or to be anomalously bright in certain bandpasses, such as Strömgren u (Grundahl et al. 1999). However, when Moehler et al. (2000) used model atmospheres with the correct iron abundance for the gravity determinations of hot HB stars in NGC 6752, they found that the "low-gravity" anomaly mostly disappeared, although a small discrepancy remained for stars with 15,000 K $< T_{\rm eff} <$ 20,000 K. Interestingly, Parise et al. (1998) also detect a possible luminosity offset of M13 HB stars in this temperature range from their 1620 Å photometry obtained with the Ultraviolet Imaging Telescope (UIT).

Although selected hot HB stars in M13 have been observed for an abundance analysis (Behr et al. 1999) and studied in Strömgren photometry (Grundahl et al. 1999), there have been no previous spectroscopic studies to obtain temperatures and gravities. Here we present spectroscopy of 22 hot HB candidates in M13 to derive $T_{\rm eff}$ and log g in order to search for any deviations from canonical HB models. We also estimate abundances of helium, magnesium, and iron. Observations of four hot HB stars in M 3 serve as a control sample.

2. Observations

We selected our targets in M 13 from the Strömgren photometry of Grundahl et al. (1998, see Table 1) and those in M 3 from the Johnson photometry of Buonanno et al. (1994, see Table 2). We also included three targets in M 13 from Behr et al. (1999) for comparison. Our targets are plotted along the HBs of M 13 and M 3 in Fig. 1. For our observations we used the Calar Alto 3.5m telescope with the TWIN spectrograph. While we observed in both channels (blue and red) the crowding and consequent stray light of the primarily red cluster stars made the data from the red channel very difficult to reduce and analyse. We will therefore limit ourselves to the discussion of the data from the blue channel. There we used CCD#11 (SITe#12a, 800×2000 pixels, (15 μm)^2 pixel size, read-out noise 6 e$^-$, conversion factor 1.1 e$^-$/count) and grating T12 (72 Åmm^{-1}) to cover a wavelength range of 3410 Å – 5570 Å. Combined with a slit width of 1.5″ we thus achieved a mean spectral resolution of 3.4 Å as determined from the FWHM of the wavelength calibration lines. The spectra were obtained on June 4–6, 1999. For calibration purposes we observed each night ten bias frames and ten dome flat-fields with a mean exposure level of about 10,000 counts each. Before and after each science observation we took HeAr spectra for wavelength calibration purposes. We observed dark frames of 3600 and 1800 sec duration to measure the dark current of the CCD. As flux standard stars we used Feige 56, HZ 44, BD+28°4211, and HZ 21.

In order to observe as many stars as possible we oriented the slit to cover up to four hot HB stars at once. This of course did not allow us to reduce the light loss due to atmospheric dispersion by observing along the parallactic angle and also required observations in fairly crowded regions.

3. Data Reduction

We first averaged the bias and flat field frames separately for each night. The mean bias frames of the second and the third night showed the same level of about 923 counts (and were therefore averaged), whereas the one from the first night had on average 877 counts. The same difference was found in the overscan regions of the respective

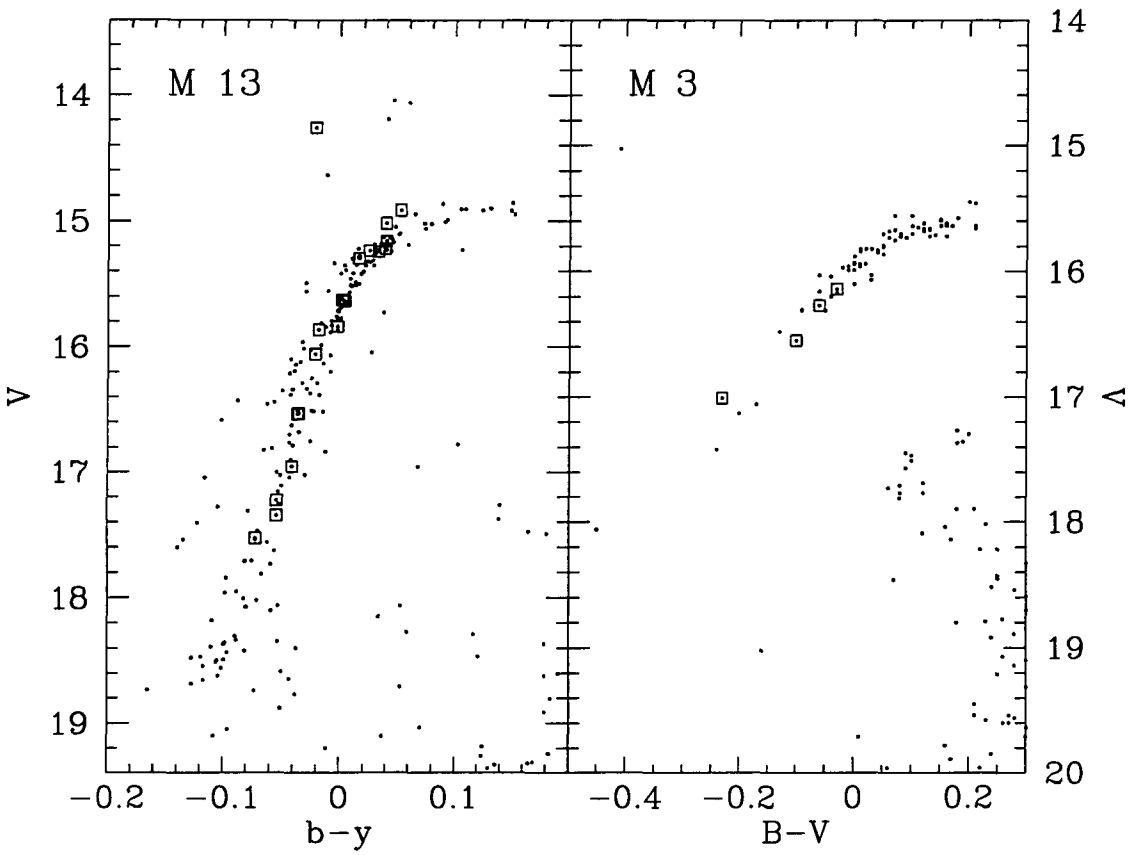

Fig. 1. The horizontal branches of M 13 (Grundahl et al. 1998, **left panel**) and M 3 (Buonanno et al. 1994, **right panel**) with the spectroscopic targets marked by open squares.

bias frames. We therefore determined the mean overscan of each science frame before deciding which bias frame to use (which was then adjusted to the individual overscan level of the science frame). The mean dark current determined from long dark frames showed no structure and turned out to be negligible (1.5±2 counts/hr/pixel).

We determined the spectral energy distribution of the flat field lamp by averaging the mean flat fields of each night along the spatial axis. These one-dimensional "flat field spectra" were then heavily smoothed and used afterwards to normalize the dome flats along the dispersion axis. As the normalized flat fields of each night differed slightly from each other we always corrected the science spectra using the flat field obtained for the same night.

For the wavelength calibration we fitted 2^{nd}-order polynomials to the dispersion relations of the HeAr spectra (using 46 unblended lines) which resulted in mean residuals of $\leq$0.15Å. We rebinned the frames two-dimensionally to constant wavelength steps. Before the sky fit the frames were smoothed along the spatial axis to erase cosmic ray hits in the background. To determine the sky background we had to find regions without any stellar spectra, which were sometimes not close to the place of the object's spectrum. Nevertheless the flat field correction and wavelength calibration turned out to be good enough that a linear fit to the spatial distribution of the sky light allowed the sky background at the object's position to be reproduced with sufficient accuracy. This means in our case that after the fitted sky background was subtracted from the unsmoothed frame we do not see any absorption lines caused by the predominantly red stars of the clusters. The sky-subtracted spectra were extracted using Horne's (1986) algorithm as implemented in MIDAS (Munich Image Data Analysis System).

Finally the spectra were corrected for atmospheric extinction using the extinction coefficients for La Silla (Tüg 1977) as implemented in MIDAS. The data for the flux standard stars were taken from Hamuy et al. (1992, Feige 56) and Oke (1990, all others) and the response curves were fitted by splines or high-order polynomials. The flux-calibration is helpful for the later normalization of the spectra as it takes out all large-scale sensitivity variations of the instrumental setup. Atmospheric disperion will cause light loss especially at blue end of the spectral range so that the flux distribution of the calibrated spectra cannot be used to infer temperatures or gravities (e.g. from the Balmer jump).

We derived radial velocities from the positions of the Balmer and helium lines. The resulting heliocentric velocities are listed in Tables 1 and 2. The error of the velocities (as estimated from the scatter of the velocities derived from individual lines) is about 30 km s^{-1}. The average

Table 1. Coordinates, photometric data, and heliocentric radial velocities for target stars in M 13 (Grundahl et al. 1998 [G]; Piotto et al. 2002 [WF3035, WF3485]; this paper [WF3085, WFPC2 data reduced as described by Dolphin 2000])

Star	α_{2000}	δ_{2000}	y	$b-y$	$u-b$	β	$v_{\rm rad}$ [km s^{-1}]
G43	$16^h41^m34^s.7$	$+36°29'13''.7$	$14^m.262$	$-0^m.021$	$+0^m.688$	$2^m.651$	-287
G129	$16^h41^m41^s.8$	$+36°29'20''.5$	$14^m.918$	$+0^m.053$	$+1^m.632$	$2^m.825$	-257
G137	$16^h41^m46^s.3$	$+36°30'12''.6$	$15^m.019$	$+0^m.040$	$+1^m.584$	$2^m.837$	-251
G195	$16^h41^m43^s.1$	$+36°30'08''.1$	$15^m.159$	$+0^m.040$	$+1^m.554$	$2^m.836$	-229
G201	$16^h41^m47^s.9$	$+36°29'47''.3$	$15^m.237$	$+0^m.025$	$+1^m.485$	$2^m.832$	-276
G208	$16^h41^m34^s.1$	$+36°29'51''.4$	$15^m.298$	$+0^m.016$	$+1^m.347$	$2^m.820$	-244
G219	$16^h41^m39^s.1$	$+36°29'54''.0$	$15^m.222$	$+0^m.039$	$+1^m.564$	$2^m.844$	-263
G235	$16^h41^m40^s.1$	$+36°29'00''.1$	$15^m.245$	$+0^m.033$	$+1^m.528$	$2^m.843$	-245
G297	$16^h41^m35^s.9$	$+36°29'27''.0$	$15^m.626$	$+0^m.002$	$+1^m.210$	$2^m.795$	-245
G314	$16^h41^m39^s.9$	$+36°30'00''.5$	$15^m.638$	$+0^m.004$	$+1^m.207$	$2^m.804$	-268
G322	$16^h41^m40^s.7$	$+36°28'52''.5$	$15^m.865$	$-0^m.018$	$+0^m.711$	$2^m.696$	-246
G342	$16^h41^m38^s.8$	$+36°30'42''.4$	$15^m.840$	$-0^m.002$	$+1^m.036$	$2^m.766$	-231
G382	$16^h41^m41^s.1$	$+36°29'39''.1$	$16^m.058$	$-0^m.021$	$+0^m.649$	$2^m.674$	-255
G496	$16^h41^m41^s.1$	$+36°30'05''.7$	$16^m.538$	$-0^m.036$	$+0^m.384$	$2^m.673$	-231
G503	$16^h41^m33^s.8$	$+36°30'15''.5$	$16^m.531$	$-0^m.035$	$+0^m.532$	$2^m.713$	-221
G635	$16^h41^m40^s.5$	$+36°31'19''.7$	$16^m.957$	$-0^m.041$	$+0^m.316$	$2^m.696$	-246
G744	$16^h41^m48^s.5$	$+36°29'59''.4$	$17^m.229$	$-0^m.054$	$+0^m.266$	$2^m.679$	-251
G781	$16^h41^m48^s.8$	$+36°29'28''.2$	$17^m.348$	$-0^m.054$	$+0^m.240$	$2^m.661$	-237
G827	$16^h41^m41^s.5$	$+36°30'37''.0$	$17^m.530$	$-0^m.072$	$+0^m.168$	$2^m.671$	-252
Star	α_{2000}	δ_{2000}	V	$B-V$			$v_{\rm rad}$ [km s^{-1}]
WF3035	$16^h41^m48^s.1$	$+36°28'20''.6$	$15^m.34$	$-0^m.01$			-288
WF3085	$16^h41^m37^s.8$	$+36°26'37''.1$	$16^m.15$	$-0^m.10$			-249
WF3485	$16^h41^m36^s.9$	$+36°26'47''.7$	$16^m.25$	$-0^m.06$			-243

Table 2. Coordinates, photometric data, and heliocentric radial velocities for the target stars in M 3 (Buonanno et al. 1994)

Star	α_{2000}	δ_{2000}	V	$B-V$	$v_{\rm rad}$ [km s^{-1}]
B254	$13^h42^m05^s.3$	$+28°25'09''$	$16^m.14$	$-0^m.03$	-151
B352	$13^h42^m28^s.8$	$+28°24'33''$	$17^m.01$	$-0^m.23$	-149
B445	$13^h42^m33^s.4$	$+28°23'57''$	$16^m.27$	$-0^m.06$	-146
B621	$13^h41^m56^s.0$	$+28°22'54''$	$16^m.55$	$-0^m.10$	-177

radial velocity of the M 13 stars of -251 km s^{-1} agrees well with the literature value of -246 km s^{-1} (Lupton et al. 1987) within the error bars. The same is true for M 3 with -156 km s^{-1} (our result) vs. -147 km s^{-1} (Pryor et al. 1988). Individual velocities may deviate considerably from the mean value because the stars may not have been in the center of the slit along the dispersion axis during the observation due to the placement of the slit to include several target stars simultaneously.

The Doppler-corrected spectra were then co-added and normalized by eye and are plotted in Fig. 2

4. Atmospheric Parameters

To derive effective temperatures, surface gravities and helium abundances, we fitted the observed Balmer and helium lines with model spectra.

We first computed model atmospheres using ATLAS9 (Kurucz 1993) and then used Lemke's version[1] of the LINFOR program (developed originally by Holweger, Steffen, and Steenbock at Kiel University) to compute a grid of theoretical spectra which include the Balmer lines H_α to H_{22} and He I lines. The grid covered the range 7,000 K $\leq T_{\rm eff} \leq$ 35,000 K, $2.5 \leq \log g \leq 6.0$, $-3.0 \leq \log \frac{n_{\rm He}}{n_{\rm H}} \leq -1.0$, at metallicities of [M/H] $= -1.5$ and $+0.5$. In Tables 3 and 5 we list the results obtained from fitting the Balmer lines H_β to H_{10} (excluding H_ϵ to avoid the Ca II H line) and the He I lines 4026 Å, 4388 Å, 4471 Å, and 4921 Å (for stars hotter than 10,000 K) with model atmospheres of different metallicity to account for possible diffusion effects (see below). To establish the best fit, we used the routines developed by Bergeron et al. (1992) and Saffer et al. (1994), as modified by Napiwotzki

[1] For a description see http://a400.sternwarte.uni-erlangen.de/~ai26/linfit/linfor.html

Table 3. Atmospheric parameters and helium abundances for our programme stars in M 3 (B) and M 13 (G, WF) as derived from fits to the Balmer and helium line profiles using metal-poor model atmospheres. Stars cooler than 10,000 K were analysed with models of a fixed solar helium abundance, using only the Balmer lines for the fit. The errors are statistical errors only.

Star	$T_{\rm eff}$ [K]	log g [cm s^{-2}]	log $\frac{n_{He}}{n_H}$
G43	13300± 550	3.00±0.10	−0.81±0.38
G129	7780± 20	2.83±0.04	−1
G137	8360± 50	3.01±0.02	−1
G195	8210± 40	2.94±0.02	−1
G201	8180± 50	2.76±0.02	−1
G208	10900± 280	3.80±0.12	−1.52±0.48
G219	8090± 60	2.82±0.02	−1
G235	7730± 30	2.70±0.04	−1
G297	10600± 190	3.64±0.09	−1.31±0.29
G314	10400± 240	3.59±0.12	−0.53±0.59
G322	15100± 550	3.76±0.09	−2.43±0.24
G342	11200± 160	3.67±0.07	−0.99±0.23
G382	13600± 290	3.64±0.05	−1.34±0.14
G496	19300± 480	4.37±0.07	−1.94±0.09
G503	15900± 760	4.13±0.12	−2.88±0.42
G635	20600± 610	4.60±0.09	−2.22±0.10
G744	21400± 910	4.61±0.12	−2.05±0.12
G781	18200±1000	4.38±0.16	−0.96±0.16
G827	21900± 600	4.88±0.09	−2.51±0.12
WF3035	7950± 80	2.58±0.17	−1
WF3085	13100± 440	3.51±0.10	−2.05±0.36
WF3485	13200± 420	3.86±0.09	−1.70±0.40
B254	10600± 150	3.62±0.07	−1.00±0.31
B352	13900± 390	3.75±0.09	−1.70±0.22
B445	9560± 150	3.22±0.10	−1
B621	12900± 340	3.83±0.09	−1.93±0.33

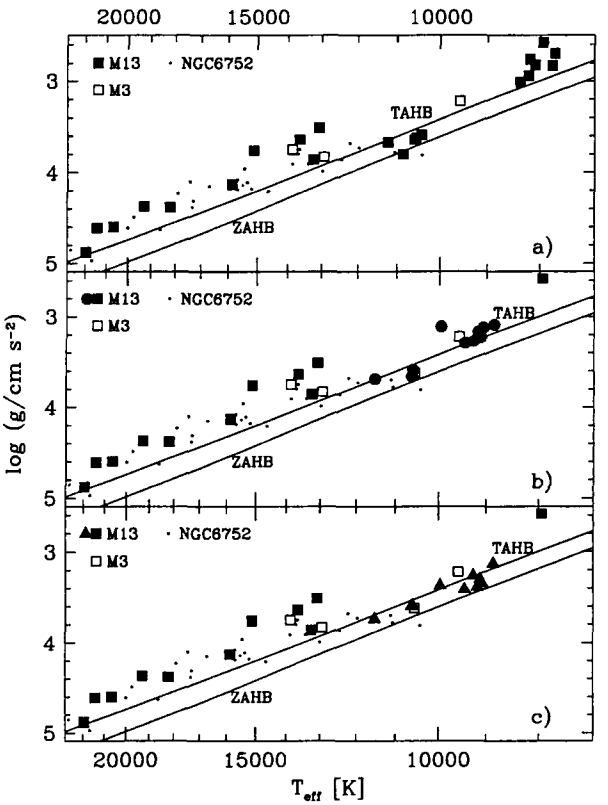

Fig. 3. Atmospheric parameters of the programme stars in M 3 and M 13 obtained with model atmospheres for the cluster metallicity ([M/H] = −1.5).
a) Temperatures and gravities for all stars are derived from fits to the Balmer line profiles.
b) Temperatures and gravities for the cooler stars ($T_{\rm eff}$ ≤12,000 K, filled circles) in M13 are derived from Strömgren photometry (see text for details)
c) Temperatures for the cooler stars (filled triangles) in M13 are derived from Strömgren photometry, while gravities are derived at fixed temperature from the Balmer line profiles (see text for details).
The solid lines mark the zero-age (ZAHB) and terminal-age (TAHB) loci of canonical HB tracks for [M/H] = −1.54. These loci define the region within which the HB models spend 99% of their HB lifetime. Also shown are the results for blue tail stars in NGC 6752 from Moehler et al. (2000) for comparison.

et al. (1999), which employ a χ^2 test. The σ necessary for the calculation of χ^2 is estimated from the noise in the continuum regions of the spectra. The fit program normalizes model spectra *and* observed spectra using the same points for the continuum definition. The errors given in Tables 3 and 5 are r.m.s. errors derived from the χ^2 fit (see Moehler et al. 1999 for more details). These errors are obtained under the assumption that the only error source is statistical noise (derived from the continuum of the spectrum). However, errors in the normalization of the spectrum, imperfections of flat field/sky background correction, variations in the resolution (e.g. due to seeing variations when using a rather large slit width) and other effects may produce systematic rather than statistical errors, which are not well represented by the error obtained from the fit routine. The rather large errors in helium abundance for stars around 10,000 K to 11,000 K reflect the strong temperature dependence of this abundance in that temperature range, where any He I lines are weak and difficult to detect. Stars cooler than 10,000 K were analysed with models of a fixed solar helium abundance.

The star G43 is found to have a high temperature ($T_{\rm eff}$ = 14,500 K) which, along with its bright visual magnitude ($y = 14^{\rm m}.26$), suggests that it is a UV-bright star. The star is clearly seen as such on the 1600 Å image of M13 obtained with the Ultraviolet Imaging Telescope (UIT, 1998), but the crowding prevents a good determination of its ultraviolet magnitude. Using the y magnitude and the derived effective temperature, and assuming an apparent distance modulus of $(m - M)_V = 14^{\rm m}.51$ toward M 13 and a reddening of $E_{B-V} = 0^{\rm m}.02$, we estimate a luminosity of log $L/L_\odot$ = 2.47. The evolutionary status of G43 is uncertain, but given the large extreme HB (EHB)

population in M13, it may be either a He-shell burning post-EHB star, or a post-early AGB star (cf. Moehler et al. 1998). In any case, since G43 is almost certainly not an HB star, it is excluded from further discussion in this paper.

As can be seen from the upper panel in Fig. 3, the stars cooler than ≈9000 K show an offset towards low gravities and appear to be separated from the hotter stars by a gap in temperature not evident from the colour-magnitude diagram. This effect has already been described by Kinman et al. (2000), who noted that some ambiguity exists in the temperature determination for stars between 8,000 K and 10,000 K because the H_γ profile at [M/H] = −1.5 for T_{eff} = 8800 K and log g = 3.0 is almost identical to that for T_{eff} = 9500 K and log g = 3.4. In order to verify the parameters given in Table 3 for the cooler stars, we redetermined their temperatures and gravities from a combination of Strömgren *uvbyβ* photometry and Balmer line profiles.

Because an empirical calibration of the Strömgren indices is not yet available for hot HB stars, we used the Strömgren indices (including Hβ) computed with the ATLAS9 code by Castelli (1998) to derive values for T_{eff} and log g. We adopted the model with [Fe/H] = −1.5 with α elements enhanced by +0.4 dex, a solar helium abundance and a microturbulent velocity of 1 km s^{-1}. The normalization of the Hβ indices by Castelli uses the values for the Sun and Vega as anchor points for a linear interpolation relating the calculated indices, β_{calc} to the observed indices, β_{obs}

$$\beta_{obs} = 1.287\beta_{calc} + 2.598 \quad (1)$$

The observed Strömgren *uvby* photometry was dereddened by E_{B-V} = 0.02, and then best-fit values of T_{eff} and log g were determined by minimizing the χ^2 difference between the observed and calculated *uvby* and Hβ photometry.

The surface gravities derived from *uvbyβ* still put the cooler stars somewhat above their expected zero-age HB (ZAHB) location, but the gap in T_{eff} vanishes (see central panel in Fig. 3). The Strömgren β index obviously measures the variations of only one Balmer line. We therefore redetermined the surface gravities by fitting the Balmer line profiles (which depend mainly on surface gravity in this temperature range) while keeping the temperatures fixed at the value derived from *uvbyβ*. The results are given in Table 4 (for stars hotter than 10,000 K also the helium lines were fitted to estimate the helium abundances) and plotted in Fig. 3 (bottom panel). The discrepancies between parameters derived solely from line profile fits and those derived from a combination of photometry and line profile fits decrease once T_{eff} exceeds 10,000 K. The stars cooler than 12,000 K in the bottom panel of Fig. 3 agree nicely with the locus of the canonical HB tracks.

For the three stars (G297, G314, G342) in M13 hotter than 10,000 K but with no evidence of radiative levitation, there is excellent agreement between the values of T_{eff} and log g derived from Strömgren photometry, and those

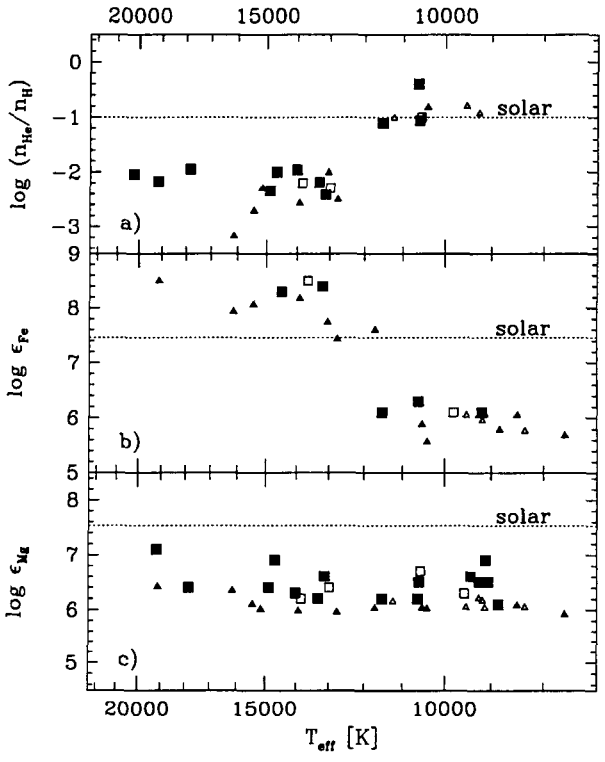

Fig. 4. Abundances of **a)** helium, **b)** iron, and **c)** magnesium for the programme stars in M 3 (open squares) and M 13 (filled squares). Also given are the results of Behr (priv. comm.) for stars in M 3 (open triangles) and M 13 (filled triangles).

derived from a detailed Balmer line fit. This agreement provides evidence in support of the Strömgren calibration of Castelli (1998) for deriving the atmospheric parameters of low-metallicity hot HB stars in this temperature range.

In Fig. 3 the stars hotter than about 12,000 K in both M 3 and M 13 show the well known offset towards lower gravities and/or higher temperatures when compared to canonical evolutionary tracks. To better illustrate this general behavior, we also give the results for the blue HB stars in NGC 6752 obtained with similar methods by Moehler et al. (2000). Note that the gravities of the blue HB stars in M 3, M 13 and NGC 6752 all follow the same trend with T_{eff}. As can be seen from Fig. 4 (top panel), the decrease in helium abundance coincides with the onset of the deviations from canonical tracks in Fig. 3.

5. Radiative levitation of heavy elements

As described in Moehler et al. (2000) and Behr et al. (1999, 2000), hot HB stars show helium depletion and iron enrichment for effective temperatures above 11,000 K to 12,000 K. To verify this behaviour from our low-resolution spectra, we fitted the iron lines in the wavelength region 4490 – 4590 Å (as described in Moehler et al. 2000). We also used the Mg II line at 4482 Å to derive magnesium

Table 4. Atmospheric parameters derived from *uvbyβ* data and Balmer line profile fits for stars cooler than 12,000 K using metal-poor model atmospheres (with solar helium abundance for those stars cooler than 10,000 K; see text for details). In the case of the M 3 stars the parameters are those derived from the Balmer line profile fits, since Strömgren photometry is not available for these stars. We also list the magnesium abundances of the stars.

Star	T_{eff} ($uvby\beta$) [K]	log g ($uvby\beta$) [cm s^{-2}]	log g (line profiles) [cm s^{-2}]	log ϵ_{Mg}
G129	8850	3.09	3.13±0.01	6.1
G137	9060	3.12	3.35±0.01	6.5
G195	9170	3.17	3.39±0.01	6.5
G201	9430	3.29	3.41±0.01	6.6
G208	9960	3.11	3.37±0.02	–
G219	9110	3.23	3.30±0.01	6.9
G235	9250	3.27	3.26±0.01	6.5
G297[2]	10590	3.59	3.61±0.01	6.5
G314[3]	10620	3.66	3.65±0.02	6.2
G342[4]	11520	3.69	3.78±0.01	6.2
B254	10600[1]		3.62	6.7
B445	9560[1]		3.22	6.3

[1] T_{eff} from Balmer line profile fits
[2]: log $\frac{n_{He}}{n_H}$ = -1.06 ± 0.23
[3]: log $\frac{n_{He}}{n_H}$ = -0.40 ± 0.43
[4]: log $\frac{n_{He}}{n_H}$ = -1.11 ± 0.16

abundances for the stars (see Tables 4 and 5). First estimates using the atmospheric parameters from Tables 3 and 4 showed that the iron abundance increases for temperatures above 12,000 K. We therefore used metal-poor atmospheres to determine the abundances in stars cooler than about 12,000 K (and the corresponding values for T_{eff}, log g, and log $\frac{n_{He}}{n_H}$). For the hotter stars we redetermined T_{eff}, log g, and log $\frac{n_{He}}{n_H}$ using model atmospheres with super-solar metallicities (see Table 5) and then repeated the abundance analysis. Since our resolution is rather low for abundance determinations, we tried to increase the S/N by averaging spectra of similar stars. For these averaged spectra we used as effective temperature the mean temperature of the individual spectra and redetermined the surface gravity and helium abundance by fitting the averaged spectrum.

The iron abundances derived from the averaged spectra are listed in Table 6. A drastic change in iron abundance between 11,500 K and 13,000 K is obvious, in good agreement with the findings of Behr et al. (1999, 2000) for hot HB stars in M 13 and M 15 and Glaspey et al. (1989) for two hot HB stars in NGC 6752. The abundances are plotted versus temperature in Fig. 4.

The iron abundance for the hotter stars is a factor of 100 greater than that of the cluster in general and in good agreement with that required to explain the Strömgren *u*-jump discussed by Grundahl et al. (1999, log ϵ_{Fe} = 8.1). We also find a one-to-one correspondence between the position of a star relative to the *u*-jump (blueward/redward) and its iron abundance (enhanced/cluster

Table 5. Atmospheric parameters and helium abundances as derived from fits to the Balmer and helium line profiles using metal-rich ([M/H] = +0.5) model atmospheres for HB stars hotter than 12,000 K in M 3 (B) and M 13 (G, WF). Also given are the magnesium abundances. The errors are statistical errors only.

Star	T_{eff} [K]	log g [cm s^{-2}]	log $\frac{n_{He}}{n_H}$	log ϵ_{Mg}
G322	14900± 450	3.89±0.09	−2.34±0.24	6.4
G382	14000± 230	3.93±0.05	−1.96±0.12	6.3
G496	17800± 440	4.34±0.07	−1.95±0.09	6.4
G503	14700± 580	4.09±0.10	−2.00±0.38	6.9
G635	19200± 640	4.56±0.09	−2.17±0.10	7.1
G744	20200±1100	4.59±0.12	−2.04±0.12	–
G781	17700±1000	4.53±0.16	−1.19±0.16	–
G827	20800± 760	4.87±0.09	−2.44±0.12	–
WF3085	13100± 330	3.66±0.09	−2.41±0.35	6.6
WF3485	13300± 320	4.05±0.09	−2.19±0.40	6.2
B352	13800± 310	3.92±0.07	−2.20±0.24	6.2
B621	12900± 270	3.99±0.07	−2.29±0.36	6.4

abundance) wherever we can determine an iron abundance (cf. Fig. 5). The mean magnesium abundance for the stars cooler than 12,000 K is [Mg/H] = −1.1 and for the hotter stars it is −1.0. So the magnesium abundance does not change during the onset of diffusion. The same result was also found by Moehler et al. (2000) for NGC 6752.

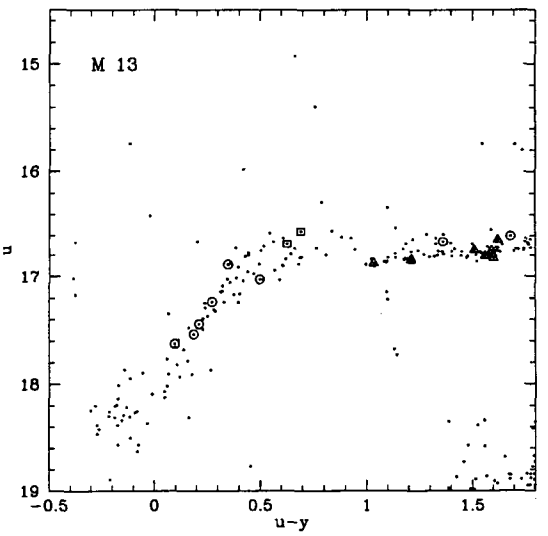

Fig. 5. The *u*-jump in M 13 with the spectroscopic targets marked: Open triangles mark stars with low iron abundance ([Fe/H] ≈ −1.5), open squares mark stars with high iron abundance ([Fe/H] ≈ +0.5). Stars for which the iron abundance could not be determined due to the limited S/N are marked by open circles.

Rey et al. (2001) have suggested that radiative levitation and helium diffusion may be responsible for the formation of a blue tail in M 13. However, we find that the HB stars in M 3 show the same abundance pattern

Table 6. Iron abundances from the averaged spectra. [M/H] is the metallicity of the model atmosphere that was used for the fit.

Star(s)	[M/H]	$T_{\rm eff}$ [K]	log g [cm s^{-2}]	log $\frac{n_{He}}{n_H}$	ξ [km s^{-1}]	log ϵ_{Fe}
G137, G195, G201, G219, G235	−1.5	9200	3.34	−1	3	6.1
G297, G314	−1.5	10610	3.67	−1	3	6.3
G342	−1.5	11520	3.74	−1	3	6.1:
WF3085, WF3485	+0.5	13200	3.86	−2.23	0	8.4
G322, G382	+0.5	14500	3.93	−2.27	0	8.3
B254, B445	−1.5	9810	3.32	−1	3	6.1
B352, B621	+0.5	13650	4.01	−2.26	0	8.5

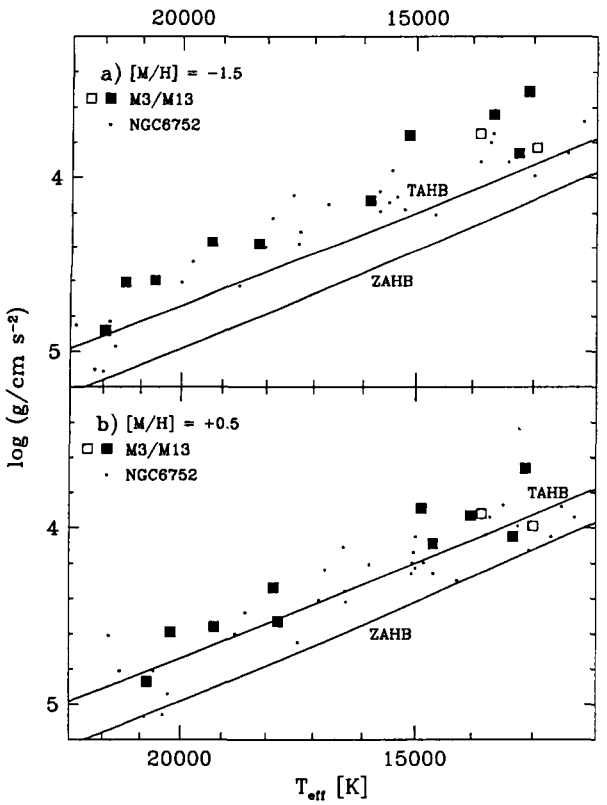

Fig. 6. Temperatures and gravities of the programme stars in M 3 and M 13 that are affected by radiative levitation. **a)** determined using model atmospheres with cluster metallicity ([M/H] = −1.5), **b)** adopting a super-solar metallicity ([M/H] = +0.5) for the model atmospheres (see Sect. 5 for details). The solid lines mark the locus of canonical HB tracks for [M/H] = −1.54. These loci define the region within which the HB models spend 99% of their HB lifetime (from Sweigart 1997b). Also shown are the results for blue tail stars in NGC 6752 from Moehler et al. (2000) for comparison.

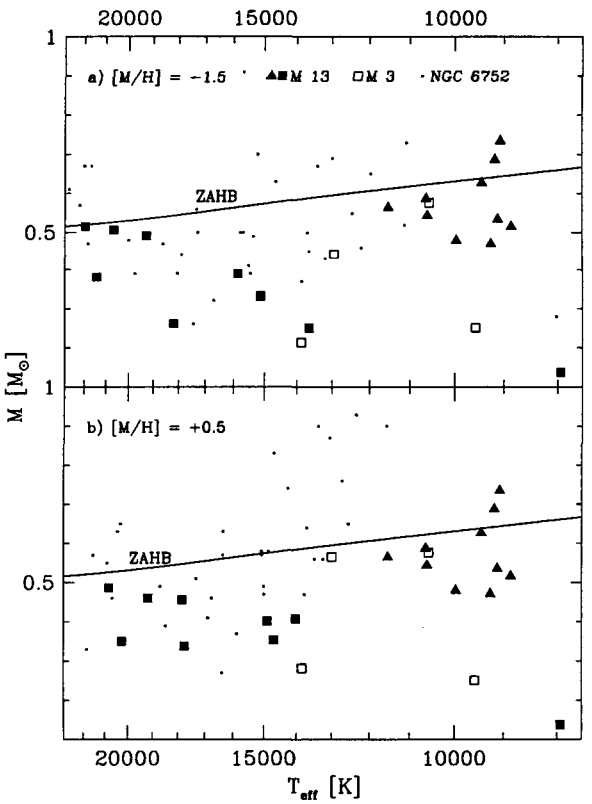

Fig. 7. Temperatures and masses of the programme stars in M 3 and M 13 **a)** determined using model atmospheres with cluster metallicity ([M/H] = −1.5), **b)** adopting a super-solar metallicity ([M/H] = +0.5) for the model atmospheres for stars hotter than 12,000 K (see Sect. 5 for details). The solid lines mark the locus of the canonical ZAHB for [M/H] = −1.54. Also shown are the results for blue tail stars in NGC 6752 from Moehler et al. (2000) for comparison.

with respect to effective temperature as the stars in M 13 and NGC 6752. The fact that M 3 contains radiatively levitated stars but does not have a blue tail provides strong evidence against the Rey et al. (2001) suggestion.

The stellar parameters derived from both metal-poor and metal-rich model atmospheres are plotted in Fig. 6 and compared to the canonical HB locus for a helium abundance Y of 0.23 and a scaled-solar metallicity [M/H] of −1.54. As already noted by Moehler et al. (2000), using scaled-solar metal-rich model atmospheres moves the stars hotter than 12,000 K closer to the canonical ZAHB,

substantially reducing the low gravity offset seen in the upper panel of Fig. 6. However, it is obvious from the lower panel in Fig. 6 that there are still discrepancies between atmospheric parameters derived from observations and the predictions of canonical HB theory.

Also, as can be seen from Fig. 7, the masses of the stars obtained from their values of T_{eff} and log g in Fig. 6 tend to be too low. Comparing the derived masses to those expected for a star on the ZAHB at the same temperature yields a mean mass ratio of 0.90 for those stars below 12,000 K with Strömgren photometry, 0.65 for the hotter stars when analysed with metal-poor model atmospheres and 0.71 for the same stars when analysed with metal-rich model atmospheres. We used distance moduli of $(m-M)_V = 14^m.51$ (M 13) and $15^m.02$ (M 3) to derive these masses.

We conclude that both the gravities and masses of the HB stars hotter than 12,000 K remain about 0.15–0.2 dex too low compared to canonical predictions even when the stars are analyzed with metal-rich model atmospheres. This remaining offset may reflect a systematic error caused by our use of metal-rich model atmospheres with scaled-solar abundances. The results of Behr et al. (1999, 2000) have demonstrated that radiative levitation can lead to severely nonsolar abundance ratios in blue HB stars. Quite possibly, the use of scaled-solar metal-rich model atmospheres may not sufficiently approximate the actual atmospheric abundances in these stars. In addition, at such a high ([Fe/H] = +0.5) metal abundance, the model atmospheres are not well tested, and are more sensitive to inadequacies in the opacity distribution function than are models at lower abundances. Another possibility, suggested by Vink & Cassisi (2002), is that an enhanced stellar wind in the radiatively levitated HB stars may alter the wings of the Balmer line profiles, leading to an underestimate of the surface gravity. While it remains to be seen if radiative levitation can be effective at the high mass loss rates obtained by Vink & Cassisi (2002), their results do raise potential concerns about the use of hydrostatic model atmospheres.

6. Effects of varying helium abundance

As mentioned in Sect. 1, M 13 shows strong abundance variations along its red giant branch, which might be attributed to either deep mixing extending into the hydrogen-burning shell (helium mixing) or pollution of the stars with the ejecta from an earlier generation of AGB stars (helium pollution). Both processes would increase the envelope helium abundance of the RGB stars with important consequences for the subsequent HB evolution. Here we discuss the potential impact of these effects on the properties of the blue HB stars in M 13.

6.1. Helium mixing

To illustrate the effects of helium mixing, we will use a set of mixed sequences computed by Moehler et al. (2000) for a main-sequence helium abundance Y of 0.23 and a scaled-solar metallicity [M/H] of −1.54. These sequences were evolved up the RGB for different amounts of helium mixing using the approach of Sweigart (1997a). Mass loss was included according to the Reimers formulation with the mass-loss parameter η_R set equal to 0.45. The evolution was then followed through the helium flash to the end of the HB phase using standard techniques. The HB locus of these helium-mixed sequences in the log g - T_{eff} plane is shown in the top panel of Fig. 8.

Since mixing increases the RGB mass loss due to a brighter RGB tip luminosity, a mixed model will arrive on the HB at a higher effective temperature than the corresponding canonical model. At the same time mixing increases the envelope helium abundance in the HB model, which leads to a higher energy output of the hydrogen-burning shell and hence to a brighter surface luminosity (Sweigart & Gross 1976).

The net effect is to shift the mixed locus in Fig. 8 towards lower gravities with increasing T_{eff} relative to the canonical locus, until a maximum offset is reached for 15,000 K < T_{eff} < 20,000 K. At higher temperatures the mixed locus shifts back towards the canonical locus, as the hydrogen-burning luminosity declines due to the decreasing envelope mass. The predicted locus along the extreme HB (EHB) does not depend strongly on the extent of the mixing, since the luminosities and gravities of the EHB stars are primarily determined by the mass of the helium core, which is nearly the same for the mixed and canonical models. Models at the cool end of the mixed locus will also differ little from the canonical models, since the cool HB stars will have undergone little mixing on the RGB. This explains why the mixed and canonical loci converge at lower temperatures in Fig. 8. Overall the variation of log g with T_{eff} along the mixed locus in the top panel of Fig. 8 mimics the observed variation. We emphasize, however, that the size of the offset between the mixed and canonical loci depends on the assumed value of η_R, becoming larger as η_R decreases (see Moehler et al. 2000).

6.2. Helium pollution

The ejecta of AGB stars which have undergone hot bottom burning should be enriched in helium (Ventura et al. 2001). Thus the pollution of either pre-stellar material or existing low-mass stars by this material will increase either the overall helium abundance or at least that in the envelopes. D'Antona et al. (2002) have studied the evolution of stars that form out of polluted material in which the helium abundance was enriched from a canonical value of $Y = 0.23 - 0.24$ to $Y = 0.29$. They found that while the effects on the pre-HB evolution are quite small, the HB morphology itself is strongly affected by helium pollution. The main effect is to shift the HB stars to hotter temperatures due to smaller turnoff masses for a given cluster age and to increased mass loss on the RGB. Polluted stars should thus be found primarily among the hottest HB stars. Indeed, D'Antona et al. (2002) suggest

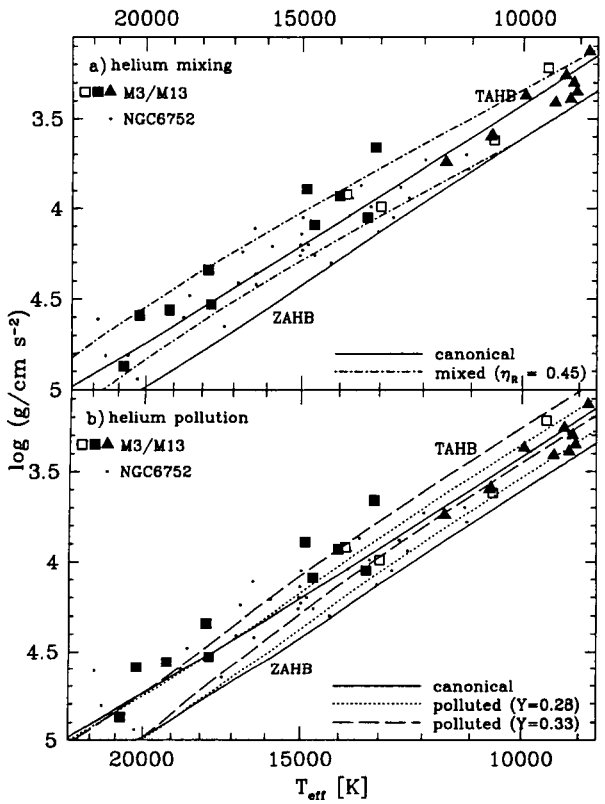

Fig. 8. Temperatures and gravities of the programme stars in M 3 and M 13 (from metal-rich model atmospheres for stars hotter than 12,000 K and metal-poor model atmospheres for cooler stars) compared to non-canonical evolutionary models. Also shown are the results for blue tail stars in NGC 6752 from Moehler et al. (2000) for comparison. The zero-age and terminal-age HB predicted by canonical models for $Y = 0.23$ and [M/H] = -1.54 are plotted as solid lines. **a)** The zero-age and terminal-age HB for [M/H] = −1.54 computed with *helium mixing* for a Reimers mass-loss parameter $\eta_R = 0.45$ (see Sect. 6.1 for details). **b)** The zero-age and terminal-age HB computed with *helium pollution* for helium abundances of $Y = 0.28$ and $Y = 0.33$ (see Sect. 6.2 for details).

that helium pollution is responsible for the extended blue tails found in such clusters as M 13 and NGC 6752.

To investigate the effects of helium pollution, we computed two additional sets of HB sequences for [M/H] = −1.54 in which the helium abundance was increased by 0.05 and 0.10 above our canonical value of $Y = 0.23$. The HB loci defined by these helium-polluted sequences are plotted in the bottom panel of Fig. 8. The gravity offset between these loci and the canonical locus is primarily due to the luminosity difference between the helium-polluted and canonical models. HB stars derive their energy from two sources: helium burning in the core and hydrogen burning in a shell. Since an increase in the initial helium abundance leads to a decrease in the helium-core mass (Sweigart & Gross 1978), the energy output of the helium core will be lower in a helium-polluted model than in a canonical model. Along the EHB, where hydrogen-shell burning is unimportant, a helium-polluted star will therefore be fainter and have a higher gravity than a canonical star. The opposite is true at cooler temperatures where the hydrogen-burning shell is a major energy source. The higher envelope helium abundance of a helium-polluted star then leads to a brighter surface luminosity and thus to a lower gravity. At the transition between the blue HB and the EHB ($T_{eff} \approx 20{,}000$ K), the gravities of the canonical and helium-polluted models are virtually identical. This is the point where the higher hydrogen-burning luminosity of a helium-polluted star offsets the lower helium-burning luminosity.

One aspect of the helium-polluted loci in Fig. 8 requires further comment. According to the helium-pollution scenario outlined by D'Antona et al. (2002), the stars at the cool end of an M 13-like HB, i.e., those near the top of the blue tail, would not be helium polluted. Thus in an actual cluster one would expect the cooler HB stars to lie within the canonical locus. However, as one goes to higher temperatures along the blue tail, the fraction of the HB stars that are helium polluted would increase, and thus the locus predicted by the D'Antona et al. scenario would shift away from the canonical locus towards the lower gravities of the helium-polluted loci in Fig. 8. This shift to lower gravities is not seen in Fig. 8, because the helium-polluted loci in this figure assume that all of the HB stars including the cooler stars are helium polluted.

6.3. Comparison with observations

In Figs. 8 and 9 we compare the effective temperatures, surface gravities and masses derived from metal-rich (T_{eff} >12,000 K) and metal-poor (T_{eff} <12,000 K) model atmospheres to the scenarios described above. While the helium-mixed models provide a better description of the temperatures and gravities derived for the hotter stars than the canonical models, they do not resolve the problem with the low observed masses. The same is also true for the helium-polluted models, where we again find that the observed masses are systematically too low. The fact that neither the helium-mixed nor helium-polluted models can account for the low masses raises doubt about the reality of any gravity and/or temperature discrepancies between the programme stars in Fig. 8 and canonical predictions. Without a better understanding of possible systematic errors, it is not possible to argue for or against the above noncanonical scenarios, given the present data.

We note, however, that the gravities of stars near $T_{eff} \approx 20{,}000$ K might potentially provide a means for distinguishing between the helium-mixed and helium-polluted scenarios. The helium-mixed models predict lower than canonical gravities at this temperature, while, as discussed above, the helium-polluted models show no gravity offset.

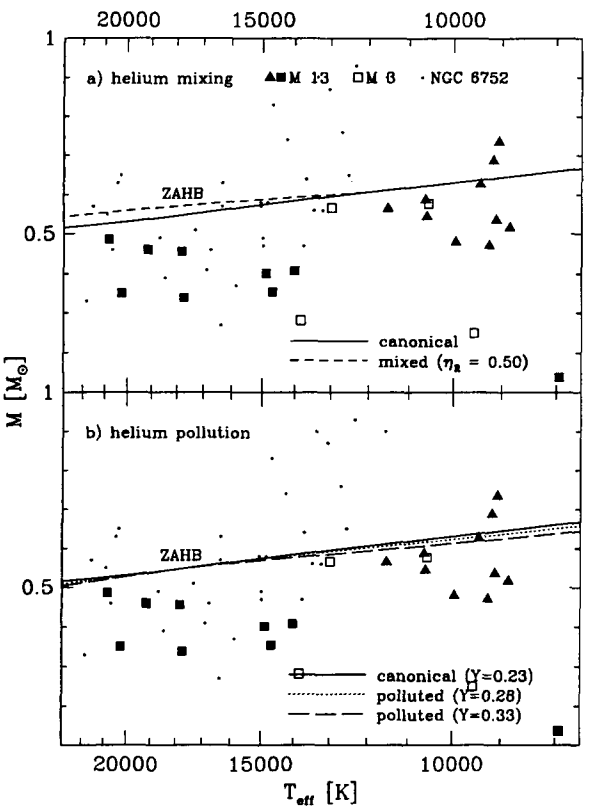

Fig. 9. Temperatures and masses of the programme stars in M 3 and M 13 (from metal-rich model atmospheres for stars hotter than 12,000 K and metal-poor model atmospheres for cooler stars) compared to evolutionary tracks. Also shown are the results for blue tail stars in NGC 6752 from Moehler et al. (2000) for comparison. **a)** Shown are the canonical ZAHB (solid line) and mixed ZAHB (short-dashed line, see Sect. 6.1 for details). **b)** Shown are the canonical ZAHB (solid line) and polluted ZAHBs (dotted and long-dashed lines, see Sect. 6.2 for details).

7. Conclusions

We have obtained low-resolution (3.4Å) spectroscopy of 22 hot HB candidates in M13, and four in M3, in order to derive atmospheric parameters (effective temperatures and surface gravities) as well as abundances of helium, magnesium, and iron. One star (G43) in M13 turned out to be a UV-bright star, while the remaining targets appear to be bona-fide HB stars. For the stars cooler than 10,000 K, there is an ambiguity in fitting the Balmer lines, due to being near the temperature of the maximum strength of the Balmer lines. However, this ambiguity can be broken by using temperatures derived from the Strömgren photometry from Grundahl et al. (1998). For the stars between 10,000 K and 12,000 K, the atmospheric parameters derived from fitting the Balmer lines and from Strömgren photometry are in good agreement.

For stars hotter than 12,000 K in both clusters, we find evidence for helium depletion and a large iron enrichment, consistent with the results on M13 by Behr et al. (1999) and on NGC 6752 by Moehler et al. (2000). The similar temperatures for the onset of radiative levitation in M3, M13, and NGC 6752 suggest that this phenomenon is unrelated to the HB morphology. Instead, the onset of radiative levitation may be connected to the disappearance of the surface convection zone, as suggested by Sweigart (2002).

We compare our temperature and gravity results with the predictions of the helium mixing scenario of Sweigart (1997b) and the helium pollution scenario of D'Antona et al. (2002). These scenarios are attractive because they can explain the origins of the HB blue tail in globular clusters such as M13 without requiring a fine-tuning of the mass loss, and because they can relate the blue tail to the observed abundance anomalies on the RGB. Both scenarios predict lower gravities (and larger luminosities) for stars near 15,000 K. For stars cooler than 12,000 K, we find the observed gravities in agreement with canonical models. This result is consistent with the work of Caloi (2001), who compared the HB luminosities of M3 and M13 to conclude that there was no evidence for a substantial surface helium abundance increase for HB stars near the temperature of the RR Lyrae stars.

For stars hotter than the onset of radiative levitation at 12,000 K, we fit the Balmer lines using metal-rich ([Fe/H] = +0.5) model atmospheres to derive the temperature and gravity. Although the use of metal-rich atmospheres reduces the discrepancy with canonical models, we still find an offset to lower gravity of about 0.2 dex, similar to what was seen at temperatures hotter than 15,000 K in NGC 6752 by Moehler et al. (2000). However, there are a couple of reasons why this result should be viewed with caution. First, the derived masses for these stars appear to be too low in either the canonical or the helium-enriched scenarios. Second, the metal-enriched atmospheres used to derive these parameters are not well-tested, and do not take into account the strongly non-solar scaled abundances. Future high-resolution spectroscopy could help reduce these possible systematic errors in gravity, by allowing the atmospheric parameters and abundances to be determined iteratively, using model atmospheres with non-solar scaled abundances.

Acknowledgements. This work was supported by the DLR under grant 50 OR 96029-ZA. We want to thank the staff of the Calar Alto observatory for their support and B. Behr for making his abundance measurements available to us. We also want to thank F. Castelli for the description of her computation of Strömgren indices.

References

Behr, B.B., Cohen, J.G., McCarthy, J.K., Djorgovski, S.G. 1999, ApJ, 517, L135
Behr, B.B., Cohen, J.G., McCarthy, J.K. 2000, ApJ, 531, L37
Bergeron, P., Saffer, R.A., Liebert, J. 1992, ApJ, 394, 228
Buonanno, R., Corsi, C.E., Buzzoni, A., Cacciari, C., Ferraro, F.R., Fusi Pecci, F. 1994, A&A, 290, 69
Caloi, V 2001, A&A, 366, 91

Cannon, R.D., Croke, B.F.W., Bell, R.A., Hesser, J.E., Stathakis, R.A. 1998, MNRAS, 298, 601
Castelli, F. 1998, MemSAI, 69, 165
Catelan, M., de, Freitas, Pacheco, J.A. 1995, A&A, 297, 345
Cavallo, R.M., Nagar, N.M. 2000, AJ, 120 1364
D'Antona, F., Caloi, V., Montalbán, Ventura,P., Gratton, R. 2002, A&A, in press, (astro-ph/0209331)
Dolphin, A. 2000, PASP, 112, 1383
Ferraro, F.R., Paltrinieri, B., Fusi Pecci, F., Cacciari, C., Dorman, B., Rood, R.T. 1997, ApJ, 484, L145
Glaspey, J.W., Michaud, G., Moffat, A.F.J., Demers, S. 1989, ApJ, 339, 926
Gratton, R.G., Bonifacio, P., Bragaglia, A., et al. 2001, A&A, 369, 87
Grundahl, F. 1999, in Spectrophotometric Dating of Stars and Galaxies, eds. I. Hubeny, S.R. Heap, & R.H. Cornett, ASP Conf. Ser. 192 (San Francisco), p. 223
Grundahl, F., VandenBerg, D.A., Anderson, M.I. 1998, ApJ, 500, L179
Grundahl, F., Catelan, M., Landsman, W.B., Stetson, P.B., Andersen, M. 1999, ApJ, 524, 242
Hamuy, M., Walker, A.R., Suntzeff, N.B., et al. 1992, PASP 104, 533
Harris, W.E. 1996, AJ, 112, 1487 (version, June, 22 1999)
Horne, K. 1986, PASP, 98, 609
Kinman, T., Castelli, F., Cacciari, C., Bragaglia, A., Harmer, D., Valdes F. 2000, A&A, 364 102
Kraft, R.P. 1999, Ap&SS 265, 153
Kraft, R.P., Sneden, C., Langer, G.E., Prosser, C.F. 1992, AJ, 104, 645
Kraft, R.P., Sneden, C., Langer, G.E., Shetrone, M.D. 1993, AJ, 106 1490
Kraft, R.P., Sneden, C., Langer, G.E., Shetrone, M.D., Bolte, M. 1995, AJ, 109, 2586
Kraft, R.P., Sneden, C., Smith, G.H., Shetrone, M.D., Langer, G.E., Pilachowski, C.A. 1997, AJ, 113, 279
Kurucz, R.L. 1993, ATLAS9 Stellar Atmospheres Program and 2 km s^{-1} grid, CD-ROM No. 13, http://kurucz.harvard.edu/
Lupton, R.H., Gunn, J.E., Griffin, R.F. 1987, AJ, 93, 1114
Michaud, G., Vauclair, G., Vauclair, S. 1983, ApJ, 267, 256
Moehler, S., Landsman, W.B., Napiwotzki, R. 1998, A&A, 335, 510
Moehler, S., Sweigart, A.V., Catelan, M. 1999, A&A, 351, 519
Moehler, S., Sweigart, A.V., Landsman, W.B., Heber, U. 2000, A&A, 360, 120
Moehler, S. 2001, PASP, 113, 1162
Napiwotzki, R., Green, P.J., Saffer, R.A. 1999, ApJ, 517, 399
Oke, J.B. 1990, AJ, 99, 1621
Paltrinieri, B., Ferraro, F.R., Fusi, Pecci, F., Carretta, E. 1998, MNRAS, 293, 434
Parise, R.A., Bohlin, R.C., Neff, S.G., et al. 1998, ApJ, 501, L67
Piotto, G., King, I.R., Djorgovski, S.G., et al. 2002, A&A, 391, 945
Pryor, C.P., Latham, D.W., Hazen, M.L. 1988, AJ, 96, 123
Rey, S.-C., Yoon, S.-J., Lee, Y.-W., Chaboyer, B., Sarajedini, A. 2001, AJ, 122, 3219
Saffer, R.A., Bergeron, P., Koester, D., Liebert, J. 1994, ApJ, 432, 351
Sarajedini, A., Chaboyer, B., Demarque, P. 1997, PASP, 109, 1321
Sweigart, A.V. 1997a, ApJ, 474, L23
Sweigart, A.V. 1997b, in The Third Conference on Faint Blue Stars ed. A.G.D. Philip J. Liebert & R.A. Saffer (L. Davis Press: Schenectady) 1997b, p. 3
Sweigart, A.V. 2002, in JD 5, XXIV IAU GA, Highlights of Astronomy, 12, in press (astro-ph/0103133)
Sweigart, A.V., Gross, P.G. 1976, ApJS, 32, 367
Sweigart, A.V., Gross, P.G. 1978, ApJS, 36, 405
Tüg, H. 1977, ESOMe 11, 7
VandenBerg, D.A. 2000, ApJS, 129, 315
Ventura, P., D'Antona, F., Mazzitelli, I., Gratton, R. 2001, ApJ, 550, L65
Vink, J.S., Cassisi, S. 2002, A&A, 392, 553

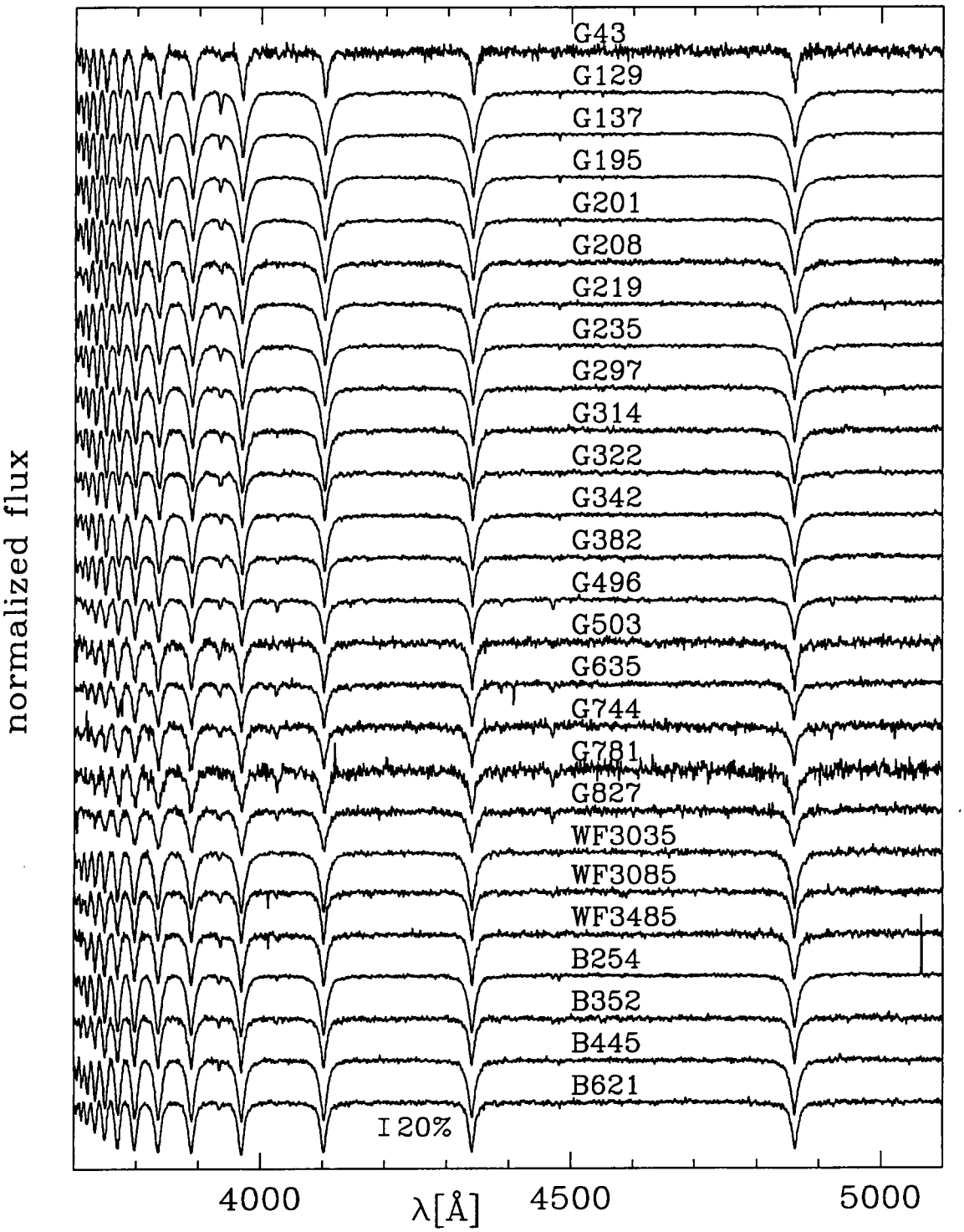

Fig. 2. Normalized spectra of the programme stars in M 13 and M 3. The part shortward of 3900 Å was normalized by taking the highest flux point as continuum value.